

Science and technology of imaging from space*

K. Kasturirangan

Imaging techniques from space, started mainly as a military reconnaissance tool, have come a long way from its early concepts to meet the present day needs of providing a precise metrology of the Earth processes and its features. The first part of the paper deals with the basic concepts of imaging from space. In this, the energy source available and the effect of atmosphere on the radiation are elaborated. Also the signatures of objects for identification and their characteristics in spatial and spectral domain are briefly touched upon. The second part of the paper deals with the challenges in realizing a satellite with limited volume and weight constraints by giving examples of very innovative approaches in the design of the optical systems for telescopes. The challenges associated with high resolution imaging and resulting high amount of data handling through appropriate data compression techniques are highlighted. The work presented here has been primarily carried out at the Indian Space Research Organization (ISRO). The paper concludes with an assessment of the futuristic direction that include improved algorithms for parameter retrieval and improved classification accuracies, improved models for atmospheric correction, new approach in artificial intelligence and expert systems for feature based classification, improved data compression techniques, ultra-light weight mirrors and adaptive optics, optical materials and detector arrays with built-in read out in the infrared region.

MODERN imaging techniques from space mainly started as a military reconnaissance tool; the earliest record of this dates back to 1793, when tethered balloons were used for obtaining visual observations. Balloons were the first 'elevated platforms' used for photography in 1858 by the French, Gaspard Felix Tournachon. Kites, doves and later manned balloons were used as platforms for photography, especially during the American Civil War. The first aerial photograph was by Wilbur Wright in 1909 using an airplane. This resulted in the use of aerial platforms for reconnaissance and imaging for strategic plan during World Wars I and II. After the war, scientists developed ingenious use of such imaging from 'heights' – especially for surveying and mapping – thus giving rise to modern aerial photography and its applications. With the advent of satellites, space-based imaging became an essential tool to look at Earth in its totality and address issues of environment, disasters, global change, natural resources management and many other applications of day-to-day relevance. Currently, all of this comes under the umbrella of 'Remote sensing' – fundamental to which is the science and technology of imaging – which has come a long way from its early concepts to modern and innovative imaging techni-

ques. Modern-day images do not just provide a visual appeal, but provide a precise metrology of the Earth processes and its features.

Why imaging from space?

Why do we go far away from Earth to understand it? As we go higher and higher we get a larger perspective coverage of the Earth, even though the details that we can discern will be less. Figure 1 shows the area of coverage from various altitudes. To study the Earth as a system, one has to understand all its features and their inter-dependence. This is possible only if we are able to see all the features together to the extent possible. In other words, we require a *synoptic view*. Apart from this there are certain features, e.g. lineaments, palaeo channels, etc. which can never be identified by observing close to the Earth.

Apart from the synoptic view, imaging from satellites has other advantages. Since the orbit of the satellite is fixed in the inertial space, as the Earth rotates, one sees newer areas during each revolution. Thus one can cover the whole globe within a certain period (Figure 2). Hence, satellite imaging enables global coverage and if we choose specific orbits like sun synchronous orbits, one can get near-identical-solar-illumination, this also helps to revisit a point on the Earth periodically. This is important to study changing phenomena like vegetative growth, snow melt run-off, etc. The repetitivity depends primarily on the swath (i.e. the width of the image strip covered) and

K. Kasturirangan is at the National Institute of Advanced Studies, Indian Institute of Science Campus, Bangalore 560 012, India. e-mail: krangan@nias.iisc.ernet.in

*Based on the Presidential address delivered by the author at the annual meeting of Indian Academy of Sciences on 9 November 2001 at Tirupati.

orbit pattern. As the swath increases, the satellite can revisit a specific location on the ground more frequently.

It is well known that as the distance of a satellite from the Earth increases, the time for one revolution of the satellite around the Earth increases. At about 35,800 km over the equator, the period of revolution of a satellite is exactly equal to that of the Earth's rotation; if the satellite is kept in the equatorial plane at that height (referred to as geostationary orbit), the satellite appears stationary with respect to the Earth. This helps to have a constant view of a part of the Earth from the satellite. Imaging from geostationary orbit helps to study weather phenomena and other episodic events like forest fire, which require constant monitoring.

Energy source for imaging

The source of energy for passive imaging from space is the radiation from the Sun. The solar radiation is nearly that of a black body at a temperature of 6000 K. However, solar radiation reaching the surface of the Earth is modified by the intervening atmosphere. When observing the Earth in visible (VIS) and infrared (IR) bands of the electromagnetic spectrum, the reflected spectrum dominates up to about $4\ \mu\text{m}$, beyond which the emission of the Earth becomes the dominant component.

Figure 3 shows the solar spectrum reflected by the Earth assuming the Sun is a black body at 6000 K. Also shown in the figure is the emitted radiation of the Earth,

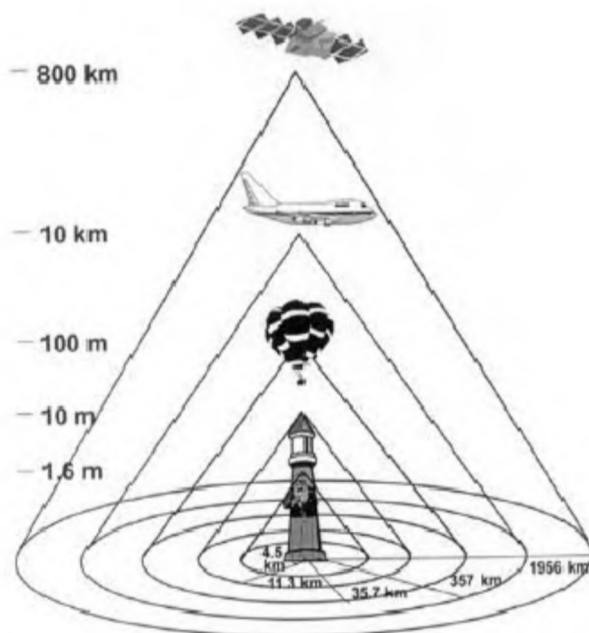


Figure 1. Typical heights of watchtowers, balloons, aeroplanes and satellites and the radius of visual coverage.

assuming that the Earth is at 300 K. Even though the peak of emission from the Earth is at $10\ \mu\text{m}$, radiation from the Earth extends into the longer wavelength microwave region where the emission is nearly proportional to the product of the emissivity and absolute temperature which is referred to as the brightness temperature.

Imaging using the natural radiation, i.e. the solar radiation reflected by the Earth or the radiation emitted by the Earth, is called passive imaging. It is also possible for an instrument to carry a source of radiation and illuminate the Earth and study the Earth's surface through its interaction with the radiation. This is called active imaging. A typical example of active imaging is imaging radars, like Side Looking Airborne Radar (SLAR) or Synthetic Aperture Radar (SAR). In this article, I restrict my discussion to passive imaging in the optical to IR region, which is used widely for Earth observations.

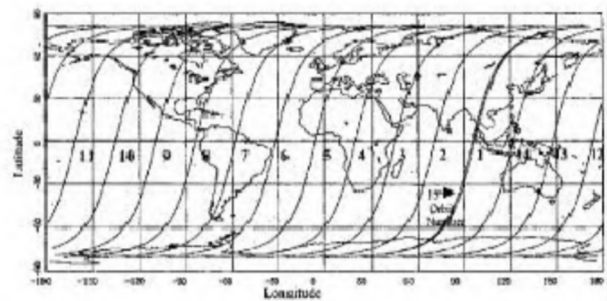


Figure 2. Descending ground traces of IRS-1A/1B for one day. The satellite crosses the equator every 103.192 min. During this time the Earth rotates a distance of 2871.8 km at the equator causing a westward drift for the ground track (1, 2, 3, ...). In 24 h the satellite makes 13.9545 revolutions around the Earth. The orbit on the second day (15th orbit) is shifted westward from orbit no. 1 by about 130 km. Ground traces repeat after every 307 orbits in 22 days.

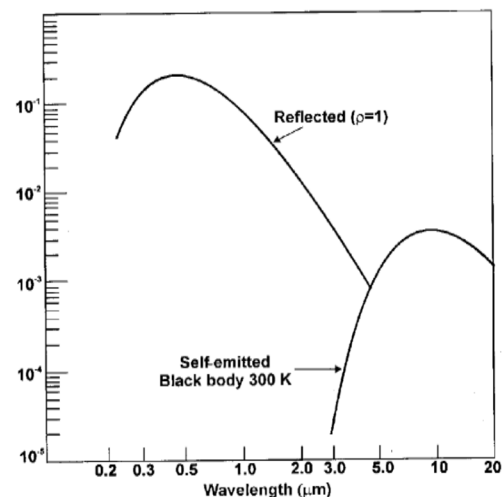


Figure 3. Energy available for remote sensing. (Atmospheric absorption not considered and microwave region not shown).

Atmospheric windows

The solar radiation, during its passage through the atmosphere, is absorbed by the atmospheric gas molecules through five major interaction processes: ionization–dissociation, electronic transition, vibrational transition, rotational transition and forbidden transition¹. These are schematically shown in Figure 4. Considering the atmospheric composition, electronic transition gives absorption lines in the ultraviolet (UV), VIS and Near Infrared (NIR) region, while vibrational and rotational transition gives absorption lines in the IR and microwave (MW) region respectively.

Apart from molecular absorption which mainly results in absorption lines, absorptions can also take place in particles. The major parameter which decides particle absorption is the imaginary part of its refractive index. Absorption by hydrometeors is particularly important in the microwave region.

Though absorption is a hindrance for remote sensing of the Earth's surface, this very phenomenon of molecular absorption is advantageously used for atmospheric sounding, since gases may be regarded as black bodies at wavelengths for which they are highly absorbing. Thus the gaseous atoms or molecules absorb and re-emit at wavelengths characteristic of the species. This characteristic radiation can be used to sound the atmosphere to get vertical distribution of temperature and concentration of the species.

Imaging is possible only in those parts of the spectrum where the atmosphere is nearly transparent. These are called atmospheric windows (Figure 5)^{2,3}. These windows are the only sources of energy for imaging. The spectral region used for imaging is generally confined to 0.4–1.3, 1.5–1.8, 2.2–2.6, 3–3.6, 4.2–5, 8–15 μm and 10 mm to 10 cm wavelength region. Among these, the first three depend on reflected solar radiation, whereas the rest are bands dependent on the Earth's emitted radiation. However, the 3–3.6 μm band will have contribution from both reflection and emission and hence is generally used at night for detection of emission.

Atmospheric scattering

Apart from absorption by gases, molecules and the other particulate matter, the radiation undergoes elastic scattering in the atmosphere. Unlike absorption, in which energy is directly removed from the beam by raising the internal energy of the atoms or molecules, in elastic scattering, spatial redistribution of energy takes place, without change in photon energy⁴. Scattering processes dominate the atmospheric effects on remote sensing in the UV and visible wavelength region and to a lesser extent in the IR. In the microwave region, scattering happens mostly with hydrometeors. The scattering cross-section and the angular scattering pattern are important factors influencing remote sensing observation.

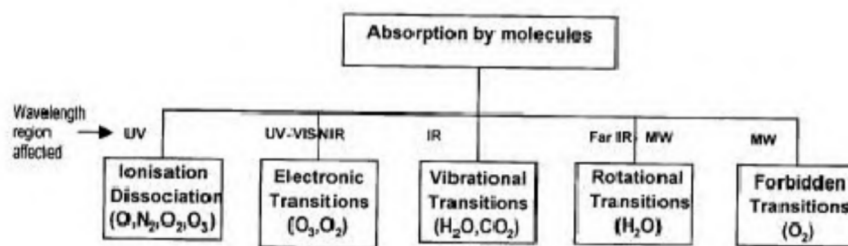


Figure 4. Major processes in the atmosphere which result in the absorption of radiation. The molecules responsible are given in brackets.

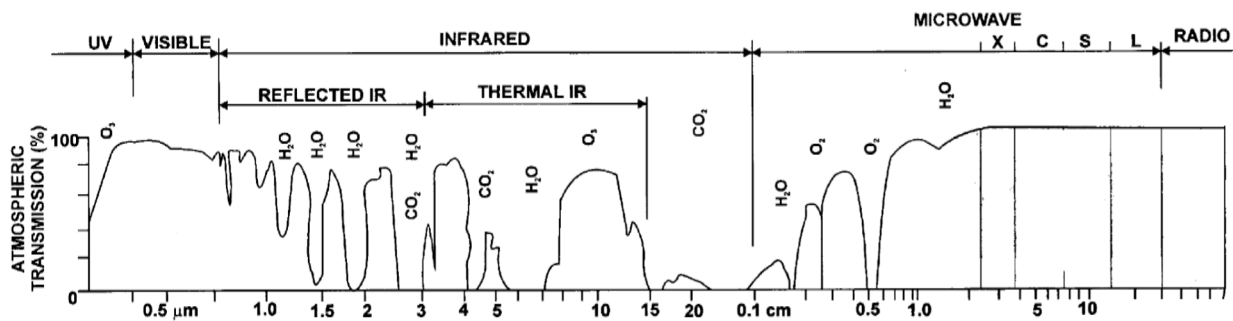


Figure 5. Atmospheric windows available for remote sensing. Gases responsible for absorption are indicated³.

The nature of scattering depends on the relative size of the scatterer with respect to the wavelength. To categorize the type of scattering, a scattering element size parameter $q = 2\pi r/\lambda$ is used, where r is the radius of the scatterer and λ the wavelength. (q essentially represents the normalized circumference of the scatterer.) There are three possibilities (Figure 6):

- (i) when $q \ll 1$, the scattering process is Rayleigh type; the scattered intensity I_θ in a direction θ (the angle between the incident and scattered flux) is proportional to λ^{-4} . The important consequence of this type of scattering is its wavelength-dependence, which shows that the lower wavelength is scattered preferentially. The actual measurement of sky radiance shows that the spectral dependence of Rayleigh scattering does not follow according to the inverse fourth power of the wavelength. One of the causes for the discrepancy is the possibility of multiple scattering, which has not been taken into account in Rayleigh's theory⁴.
- (ii) when the size parameter $q \gg 1$, geometrical optics can be applied and the cross-section can be approximated to physical size. The scattering intensity is hence independent of wavelength (sometimes referred as non-selective scattering).
- (iii) In the intermediate case when $q \sim 1$, the scattering is a complex function of λ and this regime is governed by Mie scattering. It has been observed that even in a clear atmosphere, the wavelength dependence of Mie scattering is between $\lambda^{-0.7}$ and $\lambda^{-2.0}$. The aerosol properties of importance in deciding the scattering characteristics are the size distribution, refractive index and density variation¹.

In the process of imaging, in addition to scattering and emission in the atmosphere, one has to take into account the radiation from the target under observation. This extra radiation referred to as the 'atmospheric path radiance', reduces the image contrast or in general terminology, diminishes the image sharpness. In fact, the path radiance is a 'noise', which affects the radiometric accuracy of the data.

The radiation is modified, as it passes through the atmosphere, as represented by the radiative transfer equation^{4,5},

$$\frac{dL}{ds} = -\sigma_a L - \sigma_b L + \sigma_c B + \frac{\sigma_b}{4} \int_0^{2\pi} \int_0^\pi L(\theta', \phi') p(\gamma) \sin\theta' d\theta' d\phi',$$

where

σ_a is the absorption coefficient of the medium,

σ_b the scattering coefficient of the medium,

σ_c the coefficient of emission of the medium,

B the Planck function,

$p(\gamma)$ the scattering phase function; γ the angle between (θ', ϕ') and (θ, ϕ) and (θ', ϕ') is any direction other than the direction of L .

dL/ds is the change in the radiance L as it passes through an elemental column ds in the direction defined by (θ, ϕ) , the azimuth and elevation. On the right hand side, the

first term represents loss of radiation by absorption; the second term loss of radiation by scattering, the third term addition of radiation by emission and the fourth term addition of radiation due to scattering from other directions. The sum of the third and fourth terms constitutes path radiance. In the case of imaging for wavelengths $< 5 \mu\text{m}$, atmospheric emission can be neglected and path radiance will be solely due to scattering in the atmosphere. The total detected radiation will be mainly the solar radiation directly backscattered by the target and the atmosphere, with a small contribution from the radiation in the neighbourhood of the viewing direction getting scattered into the field of view of the imaging device (adjacency effect).

In the absence of atmospheric emission, one can consider the path radiance to consist of two parts: Rayleigh path radiance and aerosol path radiance arising from Rayleigh and aerosol scattering respectively⁶. In the case of land observation, the effect of path radiance is less serious since the land surface is quite reflective and so only $\sim 5\%$ of the sensor detected radiance arises due to the path radiance. On the other hand, in the case of ocean observations, the atmospheric path radiance is significant; nearly an order of magnitude larger than the radiation from the ocean water^{7,8}. As an example, one can examine the effect of path radiance in the case of the Indian Remote Sensing Satellite (IRS) P4-Ocean Colour Monitor (OCM). Figure 7 shows the different components in the sensor radiances of the eight bands of OCM measured over the ocean. One can clearly see that the water-leaving radiance, which actually contains information on the water constituents, is only less than $\sim 10\%$ of the total signal received by the sensor^{7,9}, i.e. more than $\sim 90\%$ of the signal is the path radiance (sum of Rayleigh and aerosol path radiances), which is noise. Removing these noises is one of the major challenges in extracting data from ocean observations^{10,11}. The challenge is greater for the aerosol component of path radiance, because of larger variability and uncertainty in aerosol properties.

Signature

In imaging from space, we are interested in recognizing an object or a feature from its surroundings. To do so we

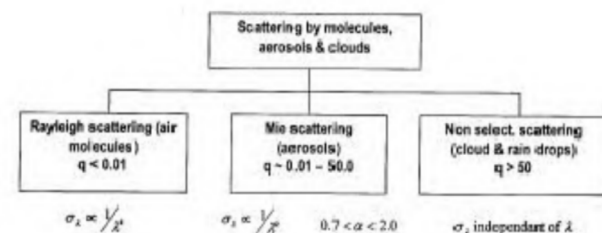


Figure 6. Major processes in the atmosphere which result in scattering of radiation. σ_s is the scattering coefficient at wavelength λ .

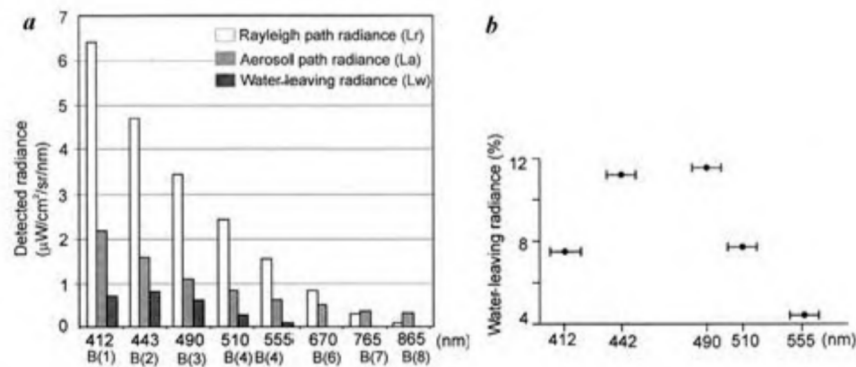


Figure 7. Radiation detected by Ocean Colour Monitor (OCM). *a*, Different components in the radiances of bands 1–8 of OCM. *b*, Percentage of water-leaving radiance in the bands 1–5 in the total detected radiances. Sensor detected radiance: $L_t = L_r + L_a + tL_w$, where t is the atmospheric transmittance.

should know what characteristic expression of the object distinguishes it from its surroundings. This characteristic feature, which forms a ‘key’ to enable an object to be identified/recognized is called signature¹². If this is achieved through the difference in the reflectance/emittance characteristics with respect to wavelength (i.e. the reflectance/emittance as a function of wavelength), then it is called spectral signature. Figure 8 shows the typical reflectance spectra of some land covers. There can be many characteristics other than the difference in the spectral reflectance/emittance characteristics, which are useful in target identification. For example, the differences in scattering cross section with respect to polarization, especially in the microwave region, provide characteristic signatures. In yet another case, if we measure the temperature using the thermal IR region, the thermal inertia could provide signatures for discrimination of certain types of objects. Temporal variation such as growth profile differences in plants can act as signatures for differentiation of crops in agricultural remote sensing; similarly, a deciduous forest shows characteristic variation in reflectance during leaf fall.

The parameters leading to signature can be quantified, thus making them amenable for computer processing. However, signatures are not completely deterministic. For example, even for the same variety of wheat and the same solar irradiance, the reflected radiance will have differences because of different leaf orientation, subtle growth characteristic-variations, etc. Thus the radiance measured is statistical in nature, with a certain mean value and some dispersion around it (Figure 9)¹².

Characteristics of image–spectral domain

Since spectral characteristics are the primary basis on which feature identification is carried out, I shall dwell upon some of the important requirements in spectral domain. These include: (i) In how many spectral bands should one take the image? (ii) Where should each band be located in the electromagnetic (EM) spectrum? (iii)

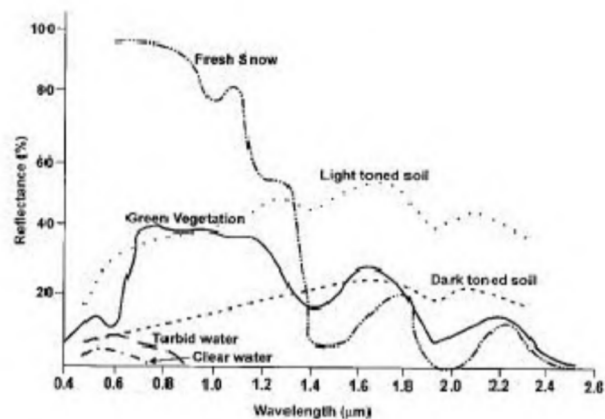


Figure 8. Typical reflectance spectra of some land covers.

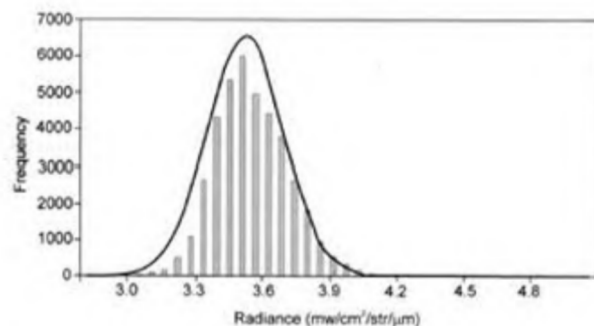


Figure 9. Frequency distribution of wheat pixels. Each pixel is identified as pure wheat by supervised classification. The continuous curve is a Gaussian fit to datasets. Data source IRS-1D/LISS-III.

What should be the spectral resolution, i.e. smallest bandwidth ($\Delta\lambda$)?

I shall discuss one of these, viz. choice of number of bands and why do we take images in several different spectral bands.

Multispectral imaging

Spectral variation is the most often used signature, especially in the optical-IR region. However, it is not easy (though not impossible) to generate continuous spectra for identifying objects. Therefore, a practical solution is to make observation in a limited number of spectral bands. One of the important considerations is, in how many bands, should the measurements be carried out to separate different classes of objects? To elucidate this point, let us consider some actual data from IRS LISS-III. We have chosen three classes—crop, water (turbid) and barren land¹². The radiance values of these are extracted from the image. (These are pure classes based on ground identification). The radiance values in the image are at times referred as DN (digital numbers), since they are transmitted as digital values or grey level values. Figure 10 *a* gives the histogram of band-3 DN values for the whole data consisting of the three classes. To separate each class from the observation of band-3 alone, the histogram should have shown distinct distribution for the three classes. It is clear, barren is distinct from the rest, while water and crop classes are mixed. Figure 10 *b* gives a similar plot for band-4 data. Here crop and barren are mixed. This simple example shows that information from a single band alone cannot distinguish all the classes. Now, we combine the information from both bands. Here, for each picture element

(pixel), the band-3 values are plotted on the *x*-axis and the corresponding band-4 values are plotted on the *y*-axis (Figure 10 *c*). Such a plot is called a scatter plot, since it represents how the DN values are ‘scattered’ in the two-dimensional space. (This is also referred to as feature space). The feature space shows that the three classes are distinctly separated, which was not possible by using either band-3 or band-4 alone. Here, we have chosen three classes to explain the concept. In practice, in a scene the number of classes is not limited to three. As the number of classes increases, the possibility of overlap between the classes increases (Figure 10 *d*), and additional bands would be required for separating the classes. With *n* number of bands, we can have *n*-dimensional feature space. However, it does not mean that separability (or in practical terms, classification accuracy) increases linearly with increasing number of bands. After 3–4 bands, for most applications, the classification accuracy only marginally increases, while the computer time requirement increases faster. In fact more than the number of bands, specific choice of band locations in the EM spectrum is crucial in feature separation for specific themes.

Characteristics of image-spatial domain

An image usually gives a two-dimensional representation. However, the principles of binocular vision can be used

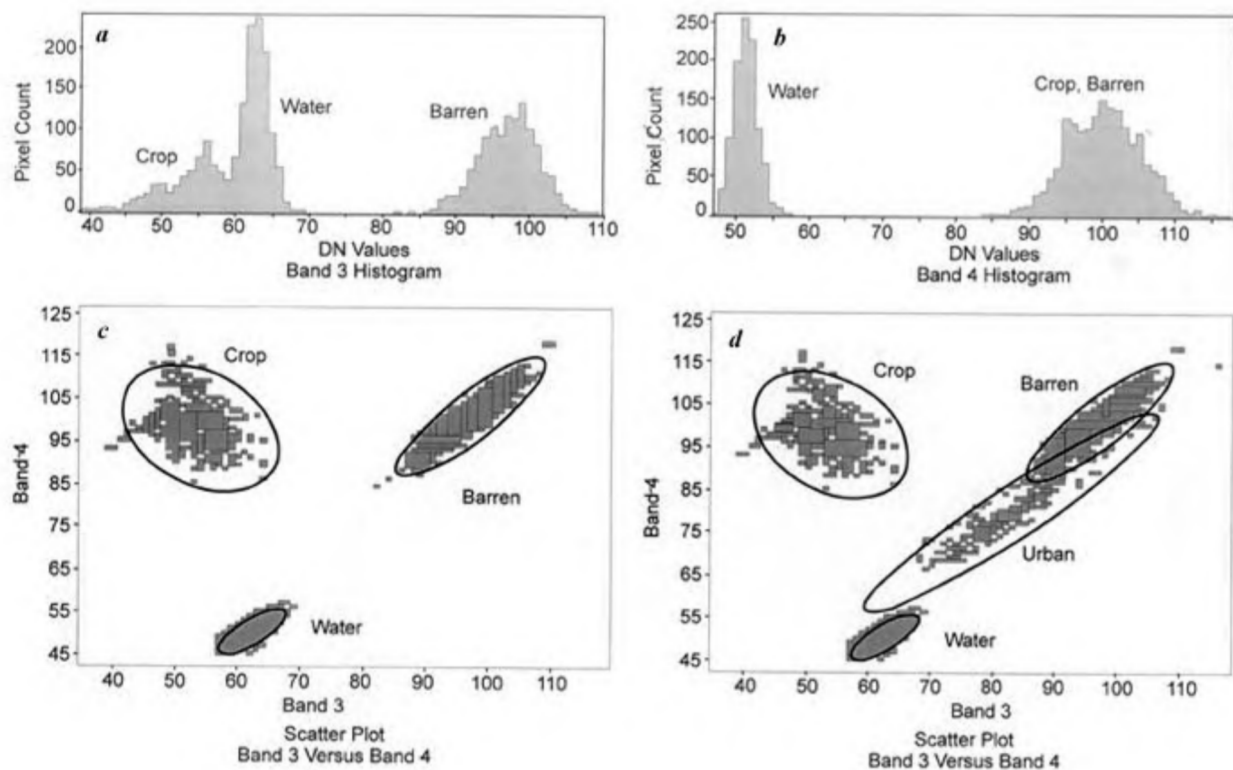


Figure 10. Schematic showing the advantage of multi-spectral imaging for class separation.

to produce three-dimensional data from images. This requires photographs of an area taken from two view angles. Conventionally, this is achieved by vertical photographs with an overlap (stereo pairs). From space various techniques are used to generate stereo pairs, such as tilting a camera to view an area from different orbits, or two separate cameras are used, each at a different angle so as to get along-track stereo pairs, or agility of the satellite is used to tilt the camera, etc. Though stereophotography is essential to generate digital elevation model, I will not dwell further on this topic.

The major parameters of importance in spatial domain are the spatial resolution and geometric fidelity of the image.

The resolution requirement¹³ generated for the visual observation (generally applicable for defence targets) is given in Table 1. Figure 11 gives an example, with res-

Table 1. Resolution requirement for visual observation

| Task | Resolution elements per minimum target dimension (line pairs) |
|----------------|---|
| Detection | 1.0 ± 0.25 |
| Orientation | 1.4 ± 0.35 |
| Recognition | 4.0 ± 0.8 |
| Identification | 6.4 ± 1.5 |

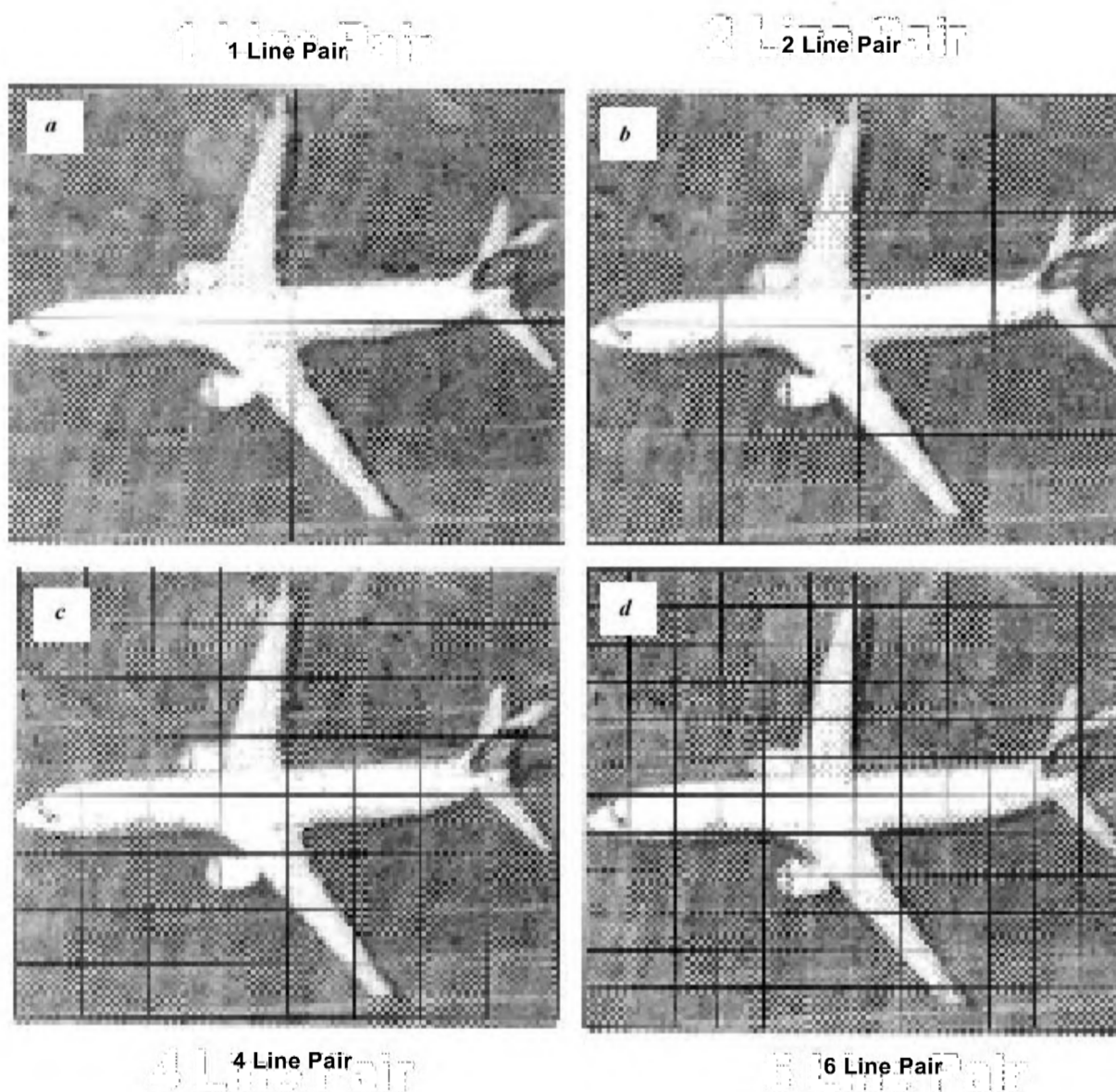


Figure 11. Schematic showing resolution improvement with respect to increased line pair.

pect to identifying an aircraft. Each square represents a pixel (or resolution element). In Figure 11 *a*, all the four pixels contain the aircraft and the background; we may say that there are no 'pure' pixels (i.e. pixels containing only aircraft). Therefore, each pixel gives radiance which is average of the target and background; this makes identifying the target difficult. As the resolution improves, larger proportion of the pixels, containing only the aircraft, increases. In Figure 11 *d*, the aircraft is covered almost by pure pixels thus enabling us to uniquely identify the target from the background. This just illustrates the significance of resolution for unambiguous feature identification. In practice, the feature detectability is critically dependent on its contrast with respect to the background. There is nothing like an ideal resolution; it depends on the application. For sea surface temperature (SST) measurements, resolution of a few hundreds of metres is adequate since SST does not spatially vary much, while for vegetative cover estimation at least a few tens of metres will be required; for urban utility planning it has to be in the metre or sub-metre class.

Imaging modes

Image can be acquired, in general, via three modes of operation¹².

Frame-by-frame

In this mode, a snapshot is taken at one instant of time covering some specific area on the surface of the target depending on the sensor characteristics and platform height. A typical example is the conventional photographic camera. The imaging carried out by area array Charge Coupled Devices (CCD) or other types of area detectors also produces images in this mode of operation (also called staring mode). Successive frames image a strip of terrain depending on the camera orientation. Generally, the successive frames are taken with certain overlap (Figure 12 *a*).

Pixel-by-pixel

In this mode, the sensor collects the radiation from one pixel (picture element) at a time. Generally, a scan mirror directs the sensor to the next pixel in the cross-track direction and by the scan mirror motion, one cross-track line of width equal to one pixel is imaged. Successive scan lines are produced by the motion of the platform. This is the way opto-mechanical scanners image. This mode of imaging is called whiskbroom scanning (Figure 12 *b*).

Line-by-line

The sensor collects radiation from one 'line' in the cross-track direction at one instant in this mode. Successive lines are generated by platform motion. Linear CCD/Photodiode arrays generate imaging using this mode. This is also called pushbroom scanning (Figure 12 *c*).

Camera design considerations

The optical system transfers the radiance from the target to the detector kept at the focal plane (Figure 13). The radiant flux (power) $\phi_d(\theta)$ delivered to the detector element is given by,

$$\phi_d(\theta) = \frac{1}{4} O_e \Delta\lambda L_\lambda \beta^2 D^2 \cos^4 \theta (W)$$

where

- L_λ is the target radiance ($W m^{-2} sr^{-1} \mu m^{-1}$),
- $\Delta\lambda$ the spectral bandwidth of the radiation to be measured (μm),
- O_e the optical efficiency – transmittance of the optical system, including atmosphere (< 1)
- β the instantaneous geometric field of view (IGFOV),
- D the diameter of the optics (m^2) and θ the angle of image location with respect to the optical axis.

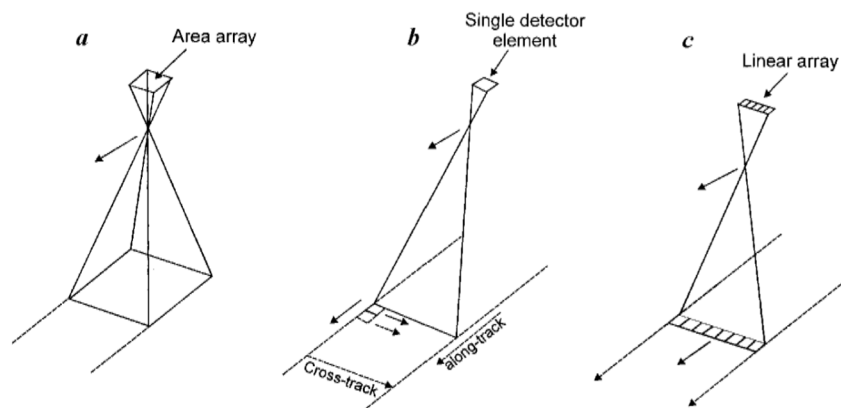


Figure 12 *a-c*. Various modes in which an image can be generated.

If the target is observed for a time τ s (usually called dwell time or integration time), then the energy $Q_d(\theta)$ received by the detector is given by,

$$Q_d(\theta) = \frac{1}{4} O_e \Delta \lambda L_\lambda \beta^2 D^2 \tau \cos^4 \theta J.$$

For improving high spatial resolution β has to be reduced. As β is reduced, to get the same energy, one has to either increase the diameter, wherein optical size increases or one has to increase $\Delta \lambda$ (which means the spectral resolutions have to be compromised) or the integration time has to be increased. Thus one sees a strong inter-dependence amongst various resolution requirements. Since realizing the best of all the resolutions critically influences the complexity of the instrument, a suitable choice for each parameter is essential.

Since the signal recorded is proportional to the dwell time, the sensor designer tries to maximize the dwell time within practical engineering limitations. In fact, maximizing the dwell time is an important consideration for the choice of the sensor type. Let us illustrate this by comparing an opto-mechanical scanner with a pushbroom sensor. If τ_o is the dwell time for an opto-mechanical scanner (having single detector element per band) and τ_p the dwell time for a pushbroom scanner, all other parameters remaining same, it can be shown¹² that

$$\frac{\tau_p}{\tau_o} = \frac{\Omega}{\beta S_{eo}},$$

where Ω is the total field of view, β is the IGFOV and S_{eo} the scan efficiency of the opto-mechanical scanner. Ω/β is the number of elements on the CCD array (across-track pixels). Thus the dwell time is considerably larger in a pushbroom scanner compared to an opto-mechanical

scanner. To illustrate a practical system, let us consider how we could realize a resolution of IRS Panchromatic (PAN) camera (5.8 m) using an opto-mechanical scanner with the type of detector and scan characteristics similar to that used in LANDSAT Thematic Mapper. It can be shown¹⁴ that for an opto-mechanical scanner with photo-diode as the detector, the signal-to-noise ratio (S/N) is such that,

$$S/N \propto \frac{D^2 \beta^3 n^{0.5}}{\Omega^{0.5}},$$

where n is the number of detector elements per band. Figure 14 gives the dependence of D on β for an opto-mechanical scanner. As can be seen from the graph, to realize 5.8 m resolution with an opto-mechanical scanner using the Enhanced TM (ETM) detector configuration and the LANDSAT orbit, the optics diameter has to be about 170 cm. The IRS PAN realized the 5.8 m resolution using the pushbroom technique using only 22 cm diameter optics (though only with 38% swath of ETM, but from a higher orbit). Hence using the same aperture of an opto-mechanical scanner, a higher spatial/spectral resolution imagery can be produced with a pushbroom sensor, without compromising S/N . This is why currently all high resolution imaging from space is based on pushbroom technology.

Electro-optical imaging system

The basic building block of an imaging system is given in Figure 15. An optical system collects the electromagnetic radiation from the scene. The choice of type of optics primarily depends on the spectral range to be covered, the

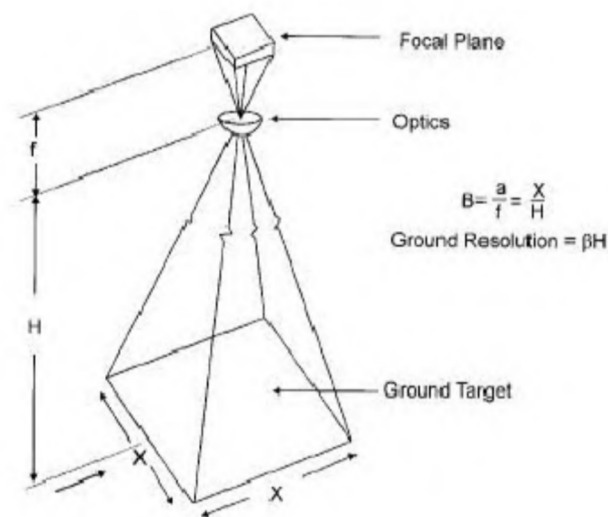


Figure 13. Imaging geometry of an optical system. The spatial resolution is βH .

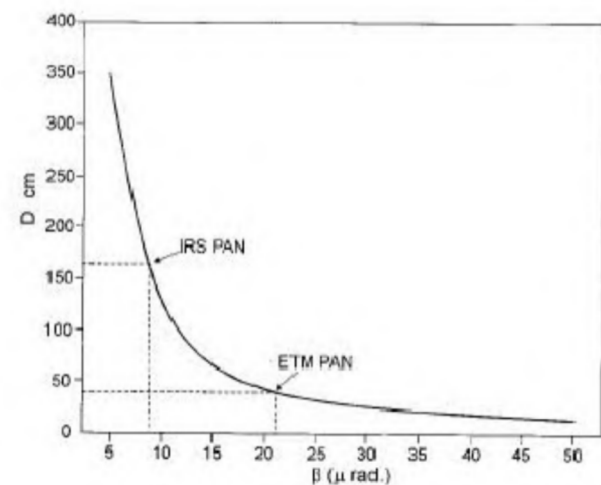


Figure 14. Variation of optics diameter (D) with IGFOV (β), to obtain the same signal-to-noise ratio, for an opto-mechanical scanner using photo-diode detectors. All other system parameters and detector characteristics are assumed to be similar to those of LANDSAT-TM.

focal length and the required field-of-view. There are various choices possible, which we shall discuss later. The energy collected has to be dispersed so that specific wavelength bands could be selected for measurement. Different types of schemes using conventional prisms/gratings, and a combination of dichroic and band-pass filters have been utilized. The major driving force is the spectral resolution requirement.

Spectrally dispersed radiation goes onto a detector which converts the electromagnetic energy to an electrical signal. The choice of the detector is important. The major driving forces are the spectral region to be covered, the ability of the detector to respond to the time variation of radiance (response time), the output voltage available for an input radiance (responsivity) and the dynamic range (which primarily is a measure of the range from the minimum to maximum signal strength the detector can faithfully record without distortion). Various types of detectors generally used include photo multipliers, photodiodes, etc. Detectors as a single element as well as linear and area arrays have been extensively used. CCDs whose spectral response covers about 0.4 to 1 μm have been the major workhorse for high-resolution imaging systems. For detecting in the thermal infrared region, mercury cadmium telluride (MCT) detectors are used. Because of the small band gap, MCT detectors are cooled to about 100 K to reduce their noise. In a spacecraft, such low temperatures are generated using passive radiation coolers, which thermally couple the detector elements to space.

The electrical output from the detector is suitably amplified, digitized and formatted and transmitted via suitable carriers. The major consideration for choice of devices and design is data transmission rate, which increases as the resolution increases. Currently, transmission is carried out via S/X bands, which limit the maximum data transmission to about 350 Mbps.

I will now give more details on one of these blocks, having chosen the optical system.

Collecting optics

There are basically three types of optical systems possible: using totally refractive elements, only reflective elements

or a combination of both, called catadioptric. The choice among these three, primarily, depends on the spectral range to be covered, the field-of-view and the aperture.

- (i) Refractive systems, because of the chromatic aberration, cover only a small spectral range to give a good performance throughout the spectral region of interest. However, using multi-element lenses, it is possible to cover a large field-of-view. Though in principle, there is no limitation on the aperture, in practice, the fabrication, mechanical support of individual elements and weight restrictions, usually limit aperture for space use to about 6–8”.
- (ii) Since there is no chromatic aberration, reflective optics can cover a large spectral range from UV to far IR. Large aperture size is also possible. But the field-of-view, especially for the on-axis system, is limited to fraction of a degree. However, all reflective off-axis systems have been realized to have field-of-view extending to a few degrees.
- (iii) The smaller field-of-view limitation of reflective system is taken care of in the catadioptric system, wherein lens correctors are used at suitable locations in the optical path. However, due to the introduction of the refractive element, the spectral range is limited.

In the IRS system we have been using all the three types of collecting optics. LISS-I, II and III use refractive optics, while the PAN and Cartosat-1 are off-axis all-reflective telescopes. IRS-1C PAN was the first off-axis optical system configuration to be used for Earth observation from space. For long focal length systems, the three-mirror off-axis system is less compact. Therefore, Technology Experiment Satellite (TES) and the future Cartosat-2 use on-axis system, with refractive correctors to increase the field-of-view.

Optics fabrication

The increasing cost per kilo of launching payloads into space demands reducing the weight of all subsystems of the satellite. Thus large space-borne mirrors are required to be lightweighted, maintaining at the same time low levels of stress and low deflections due to static and dynamic loads. The surface deformation should be extremely

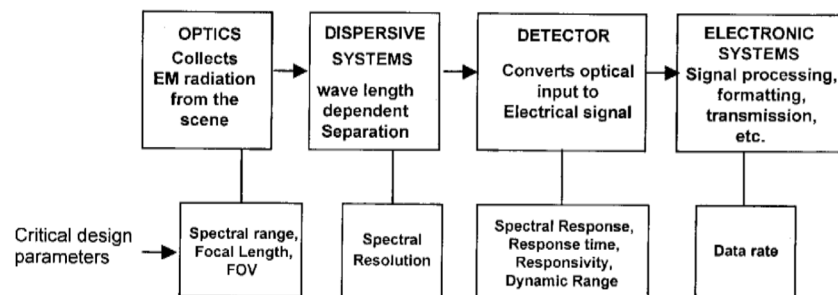


Figure 15. Basic building block of an electro-optical imaging system.

small to satisfy the performance during operation and the natural frequency should be high enough to avoid any coupling with excitation during launch.

In order to overcome the problem of increased mass, large mirrors are generally weight-relieved by scooping out the material in such a way that the mass is removed without sacrificing the stiffness significantly (Figure 16). For a lightweight mirror design variables in terms of structural parameters are overall thickness (t), face-plate thickness (t_p), cell-wall thickness (t_c), effective cell spacing (B) and cell width (H). The lightweighting pattern should maximize the bending inertia to reduce the deflection while keeping the other parameters as low as possible. The lightweight pattern should also result in low dynamic stresses and high natural frequency.

Generally, for high accuracy, the mirror is modelled using a finite element software such as NASTRAN with different elements like solid element, a plate/shell element or a beam element, as applicable. Design is optimized for the above parameters by determining appropriate values of design variables such as face-plate thickness, cell-wall thickness of scooping, etc. As an example, the IRS Cartosat-2 payload telescope mirror (about 700 mm diameter) had an original weight of 74 kg, which was reduced to 30 kg according to the above-mentioned procedure.

In practice, techniques such as water jet/CNC (computerized numerical control) milling are adopted by which cavities are ground into the rear of the mirror, thus producing a structure according to the design. The lightweight mirror cannot be polished by conventional processes. Thus fabrication of lightweighted aspherics requires synergy of advanced technologies based on CNC profil-

ing, finite element method, supported wiffle tree support for countering the gravity sag effects and precision interferometric diagnostic tools. Depending on the amount of material to be removed from the nearest spherical surface, the required aspherization can be carried out either at the grinding stage or at the polishing stage. For large aspherical surfaces, where the amount of material to be removed is more than 100 μm , the state-of-the-art technique is to first generate the required aspheric profile using grinding techniques and then polish the surface using full size flexible polishing plates without any high-frequency residual spatial defects. Finally, the mirror is re-polished to remove the residual defects by the computer-controlled polishing technique. A more advanced technique is ion-beam polishing. This has to be carried out in a high vacuum system as a final touch up.

There are many more techniques like float polishing, neutral ion beam figuring, plasma-assisted chemical etching, ductile grinding, etc. which will remain a challenge for the optic industry, for rapid and economic fabrication of large optical components. A parallel approach is lightweighting by water-jet milling and subsequently fusion welding of face plates, followed by CNC profiling and ion-polishing.

While selecting the mirror materials, the properties of importance are thermal expansion coefficient, polishability, mechanical stiffness and long-term stability. For example, for space optics low coefficient of thermal expansion is required to avoid misalignment of the optics, distortion of optical elements and variation of focus. Considering these properties, the two materials that are widely in use are Schott's Zerodur and Corning's ULE silica (7971). New materials like silicon carbide and its variants, and metal matrices and their derivatives are supplementary/complementary to matured low expansion glass and beryllium materials.

For refractive optics, the refractive index stability is important for thermo-optical stability and should be as low as $1 \times 10^{-7}/^\circ\text{C}$, for which a variety of optical materials are available and under continuous improvement by many manufacturers.

The mechanical materials that are normally used to hold/house the optical components, should be judiciously selected, so as to have high degree of thermal compatibility with that of optical materials. A theoretical analysis is carried out in order to find out the type of mechanical materials and the mounting configuration, which impart only allowable stress under thermal variation, so as to keep system modulation transfer function (MTF) independent of temperature change. Temperature stability is achieved using low expansion materials like Invar, in which case, the penalty has to be paid in terms of specific weight. When weight has to be controlled, carbon fibre composites are used for telescope tubes and associated structures.

Surface figure error, surface irregularity and surface micro roughness are the residues left on the optical sur-

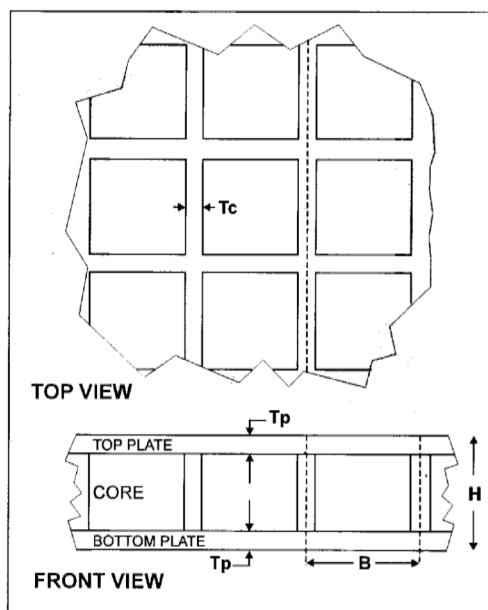


Figure 16. Schematic of lightweighting of mirror with square core.

face after fabrication. Surface figure error is defined as mismatch with respect to ideal surface. Surface figure contributes to the formation of the central core of the airy disc. To a certain extent, this error can be compensated in the integrated optical system. Surface irregularity is the undulation on the optical surface over a length of millimetres. Surface irregularity contributes to small angle scatter. Being a random phenomenon, it is not possible to compensate in the integrated system. The surface irregularity essentially degrades MTF, with respect to the theoretical value depending on the magnitude of undulation. MTF degradation due to various levels of surface irregularity (in terms of peak-to-valley (PV) ratio) can be computed using Shannon's empirical relationship given by¹⁴:

$$\text{MTF} \sim 1 - (W_{\text{PV}}/0.63)^2 [1 - 4(X - 0.5)^2] \text{MTF}_{\text{diff.lim.}}$$

where W_{PV} is peak-to-valley wavefront error in λ and X is normalized spatial frequency. $\text{MTF}_{\text{diff.lim.}}$ is the MTF of a diffraction limited system. This is graphically shown in Figure 17.

Surface micro-roughness is a high frequency undulation ranging over less than a fraction of a millimetre. This is also a random residue and hence it is not possible to compensate for it in the integrated system. Micro-roughness contributes to wide-angle scatter. Contribution from micro-roughness is appreciable for shorter wavelengths of the electromagnetic spectrum.

Wider spectral coverage of the telescope system in the visible NIR regions calls for innovative design and development techniques to improve the spectral range reflector coatings. The enhanced aluminium multilayer mirror-coating technology is currently used in the visible and IR regions. The existing technology for enhanced aluminium mirror-coatings on medium- and large-sized optical components may be replaced in future by techniques of ion-assisted deposition to enhance the packing density and morphology.

Indian Space Research Organisation (ISRO) has established modern technologies for design, fabrication and testing of large aperture, lightweight optical systems necessary to meet the challenges of high-resolution, space-

borne imaging applications. However, to meet the future requirements of ultra lightweight optical systems to be used in highly agile spacecrafts on-board, where optics needs to be an order of magnitude lighter in weight than that being realized currently, it is necessary to look beyond current technologies of materials, design and fabrication of space-borne large-aperture optics. The directions for future development include foam-based silicon-carbide large-area mirrors of 5 kg/m^2 area density with nanosurface engineering technologies adopting ion/laser systems and multi-layer high reflection coatings and associated adaptive techniques for real-time imaging corrections.

Telescope realization

Mechanical design

Mechanical design of the telescope involves designing of mirror mounts subassembly, detector head subassembly and a housing structure on which various subassemblies are mounted at desired locations. Main requirements for the mechanical design are dimensional stability and survivability of the subassemblies and their components under thermal, launch and assembly loads. Thermal loads arise due to change in environment temperature at the ground and in space. These temperature variations induce thermal stress in the optical components due to difference in coefficient of thermal expansion (CTE) of optical components and the mounting materials. Mechanical design should take care of survivability of the optical components under such temperature variations. Temperature changes in the operating conditions also affect the dimensional stability of the telescope. Temperature change causes changes in the dimension of the mechanical housing, which in turn can disturb the alignment of the telescope. This change in temperature would also degrade surfaces of the optical components due to difference in the CTE of two different materials.

Launch loads come in the form of sine and random vibrations. Mechanical design should take care of the survivability and dimensional stability of the optical components under such launch loads.

The other type of load which can deform the optical surfaces are the assembly loads which arise during the process of assembly of the optical component onto the respective interfaces due to lack of flatness of the interfacing surface. Therefore, mechanical design should take care that not only the optical components should survive launch loads but also that the deformation of the optical surfaces should be minimum under assembly loads.

Problems arising due to thermal, launch and assembly loads can be taken care of by proper combination of flexibility and stiffness in the design of optical mounts and having optimum number of fixing points for the sub-assemblies.

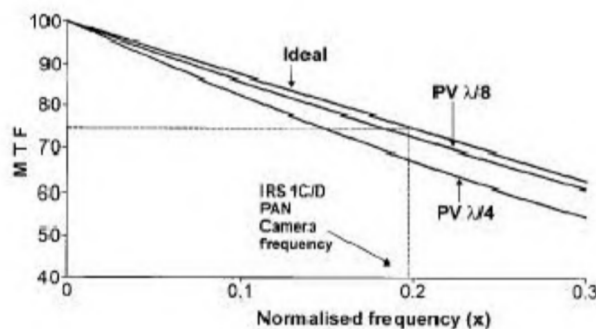


Figure 17. MTF degradation due to surface irregularity.

Gravity affects the dimensional stability of the telescope in two ways. It deforms the optical surfaces and disturbs the alignment of the telescope. The telescope is aligned under the effect of gravity on the ground. When it is operating in space having no gravity effect, this change in gravity causes change in the aligned positions of the different subassemblies. Mechanical design should take care to minimize these problems by providing sufficient stiffness to the housing structure. Deformation in the mirrors can be taken care of by scooping the mirror from the backside to give high stiffness-to-weight ratio.

In case the housing structure is made out of a material like carbon fibre reinforced plastic (CFRP), moisture gets absorbed at the ground due to humidity present in the environment, which causes dimensional changes of the housing structure. This moisture evaporates in space, which affects the alignment of the telescope due to shrinkage of the housing structure. Special surface treatment and specialized resins are used to minimize humidity effect on the CFRP structure used for telescope fabrication.

Optical alignment

The alignment of various optical elements is a major task, in order to realize an optical system with image quality according to the design. To start with, the components are mounted and aligned to an accuracy possible due to mechanical fabrication. This will generally place the components within about 100 μm , and arc minute accuracy in positioning and tilt. The residual misalignment produces aberrations of the final image. A point source after passing through an ideal (perfect) optical system, generates converging wavefronts that are spherical. Any aberration is manifested as departure of the wavefront from sphericity. Therefore, if we measure the shape of the converging wavefront, we can estimate the aberration. This is achieved using an interferometer. The prime focus of the telescope to be aligned is kept at the focus of high quality converging wavefront generated by the interferometer. The emerging wavefront is retro-reflected to the interferometer by a high quality reference flat (Figure 18). Interference takes place between the retro-reflected test

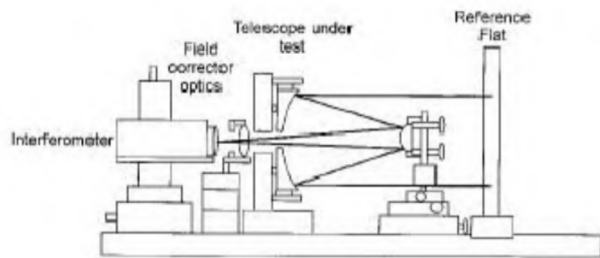


Figure 18. Configuration of telescope alignment using interferometer.

beam and the high quality reference beam generated by the interferometer. Null fringe (Figure 19 a) forms if the telescope is free from aberrations. Null fringe is sensitive to external disturbances. Therefore, for all practical purposes, the interferogramme is acquired with a slight tilt and hence appears as straight line fringes (Figure 19 b).

Misalignment in the telescope produces aberrations in the test wavefront which get manifested in the interferogramme. Typical interferogramme for some of the optical aberrations, namely astigmatism and defocus are also shown in Figure 19. The interferogramme obtained is generally caught on a video camera and stored on a computer for further analysis. An optical path difference map is generated from the interferogramme, thereby generating the wavefront shape. The wavefront shape is expressed in terms of Zernike polynomials, which are represented as¹⁵:

$$w(r, \theta) = \sum z_i P(r, \theta),$$

$$w(r, \theta) = \sum_{n=0}^k \sum_{m=0}^n z_{nm} r^{n-2m} \begin{bmatrix} \sin \\ \cos \end{bmatrix} \{(n-2m)\theta\},$$

sine function when $n - 2m > 0$, cos function when $n - 2m \leq 0$,

where the number of Zernike coefficients, $k = [(l + 1)(l + 2)]/2$; l is the degree of the polynomial, r, θ are the polar coordinates of the wavefront at the exit pupil, and n and m variables.

The Zernike polynomials were developed as a convenient set for representing the wavefront aberrations over a circular pupil. The main advantage of expressing wavefronts in terms of Zernike polynomials is that they can be correlated with the classical optical aberrations.

The Zernike polynomials are orthogonal over the circular pupil of unit radius. Inclusion or exclusion of any of the polynomial coefficients, does not affect other polynomial coefficients since they are independent of each other. This property allows one to evaluate the wavefront by eliminating some of the coefficients, namely tilt, defocus, etc. Knowing the sign and magnitude of the aberrations helps in re-optimizing one or more number of optical elements of the telescope.

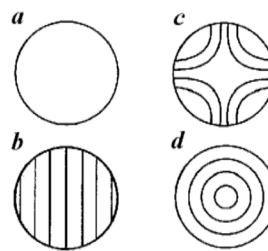


Figure 19. Fringe patterns under various misalignments. a, Ideal plane surface; b, Tilt between reference and test surface; c, Astigmatic fringe (due to tilt/decentre); d, Defocus.

Image quality evaluation

How does one evaluate the quality of the image? We know a parallel beam incident even on an ideal aberration-free lens produces energy distribution due to diffraction. This is called the point spread function (PSF), which has a central maximum containing about 84% of energy, followed by a series of maxima and minima (Figure 20 *a*). For an optical system which does not produce the diffraction limited image, the shape of the curve will be such that the energy contained in the central maximum will be reduced and the energy gets redistributed to the surroundings (Figure 20 *b*). How energy gets redistributed compared to the ideal diffraction limited image is a measure of the quality of the image. However, the PSF is not convenient for use in evaluating a practical system. What generally one uses for an imaging system is to find out how the system reduces the contrast of the object from the object space to the image space due to the energy spread, which is referred to as Modulation Transfer Function (MTF). Mathematically, Fourier transform of the PSF gives an optical transfer function, which has phase and magnitude. Since we are dealing with incoherent imaging, only the magnitude of the MTF is relevant to us. As an illustration, one may note that the contrast modulation (C_m) of black-and-white target is given by

$$\frac{L_{\max} - L_{\min}}{L_{\max} + L_{\min}}$$

Table 2. Zernike polynomial coefficients and corresponding misalignments

| Term no. (Z_i) | Zernike polynomial | Corresponding misalignment |
|-----------------------|---------------------------|-----------------------------|
| Z_1 | $r \cos \theta$ | Tilt about x-axis |
| Z_2 | $r \sin \theta$ | Tilt about y-axis |
| Z_3 | $2r^2 - 1$ | Focus shift |
| Z_4 | $r^2 \cos 2\theta$ | Astigmatism at 0/90 deg |
| Z_5 | $r^2 \sin 2\theta$ | Astigmatism at ± 45 deg |
| Z_6 | $(3r^2 - 2r) \cos \theta$ | Coma x |
| Z_7 | $(3r^2 - 2r) \sin \theta$ | Coma y |

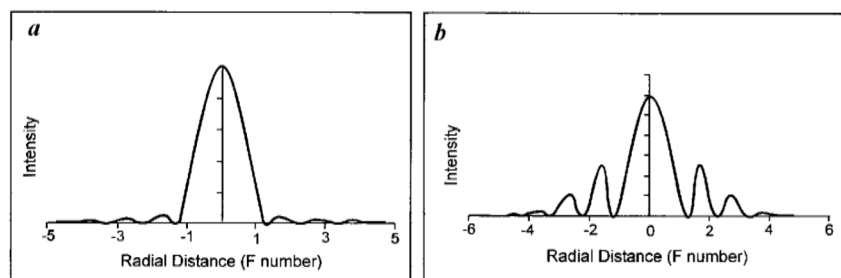


Figure 20. Point spread function for a circular aperture. *a*, Diffraction limited system and *b*, Aberrated system.

(Figure 21). MTF is the ratio of the contrast modulation of the image to the contrast modulation of the object.

The advantage of using MTF is that each component of the imaging system can be designed to have a specific MTF value and the overall system MTF is the product of the MTF values of the components. That is,

$$MTF_{\text{camera}} = MTF_{\text{optics}} * MTF_{\text{detector}} * MTF_{\text{platform motion}} * \dots$$

Any obscuration at the entrance aperture reduces the MTF. MTF at various normalized spatial frequencies for unobscured and obscured systems ($\epsilon = 0.3$ and 0.8) is shown in Figure 22. For an obscured system, diffraction takes place at the outer circle as well as the inner opaque circle. Therefore, the diffraction of an obscured system is the convolution of the diffraction of the outer and inner circles. Due to this, the radius of the first minima of the airy disc decreases with increasing obscuration ratio, affecting the MTF.

High resolution imaging

There is a constant demand for getting better and better spatial resolution, which poses a great technological challenge. Let us review some aspects related to this. As discussed earlier, as spatial resolution increases IGFOV is reduced. For the same detector size, this implies that one should have a long focal length system. In addition, increased energy collection also calls for new techniques to increase the dwell time. Some of the associated issues are:

- Long focal length optics calls for larger diameter optics, which in turn has fabrication issues, weight and volume penalty. Currently, efforts are on to make ultra lightweight large diameter optics using silicon carbide (SiC) faceplates sandwiched between SiC sponge to have adequate stiffness.
- To achieve a manageable optical size, we require longer integration time. This could be achieved by Time Delay and Integration (TDI) devices, wherein the same area is sequentially observed a number of times (using multiple arrays) and the signals are added. If there are ' n ' stages of TDI, one gets an improvement in S/N by square

root n compared to a single array (signal adds in phase, but noise in quadrature).

The second method is to reduce the sub-satellite velocity by rotating the camera view angle in the opposite direction – step and stare. IRS TES, employs this technique to realize 1m resolution imagery from 600 km altitude.

As spatial resolution increases, the data rate also increases. There is a limit on the maximum data rate that can be transmitted due to available bandwidth on the data transmission channel. Various techniques used to tackle this problem include

(i) storing the data for a certain duration to an on-board recorder and playing it for a longer time to transmit. The transmission rate reduction is by the ratio of recorded time to read-out time;

(ii) transmitting to a geostationary satellite by optical links, storing and transmitting for a longer duration, and

(iii) adopting suitable data compression techniques.

We shall discuss some aspects related to data compression in the next section.

Data compression

A common characteristic of most images is that the neighbouring pixels are correlated and therefore contain certain amount of redundant information. Following are three possible types of redundancy¹⁶. The fundamental approach for compression is to reduce redundancy.

- Spatial redundancy or correlation between neighbouring pixel values.
- Spectral redundancy or correlation between different colour planes or spectral bands.
- Temporal redundancy or correlation between adjacent frames in a sequence of images (in video applications).

In an ideal case, the compressed data after decompression should have the same DN value for each original pixel. Then the compression is said to be loss-less. However, loss-less compression can achieve only a modest amount of compression (< 2)¹⁷. To have greater data compression, one has to resort to lossy compression. An image reconstructed following lossy compression will have certain degradation relative to the original image. The remote sensing satellites, viz. SPOT series (French satellites), IKONOS (USA satellite) use on-board data-compression techniques to reduce the data-transmission rate. The forthcoming Indian remote sensing satellites – Cartosat series will be using JPEG-like compression for data transmission. The error generated due to compression is dependent on the complexity measure of the image and the sophistication of the compression algorithm used. A generally

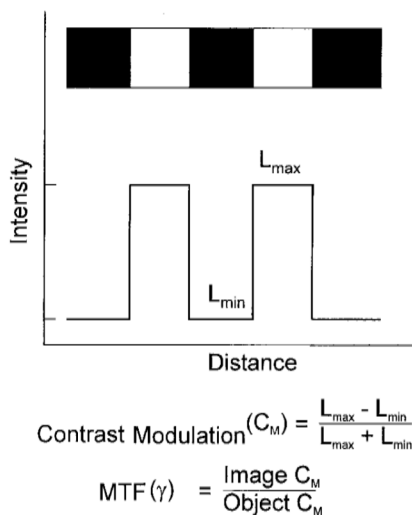


Figure 21. Schematic illustrating contrast modulation. L_{\max} and L_{\min} are the maximum and minimum radiance recorded.

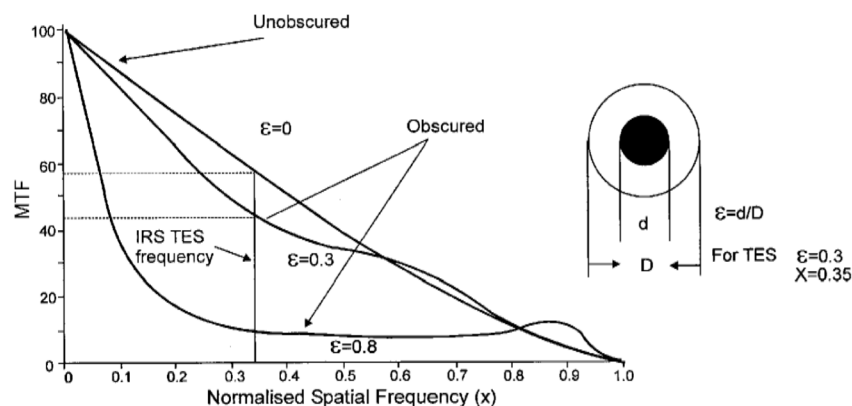


Figure 22. Diffraction limited MTF for various obscuration ratios of ϵ , which is the diameter of the central obscuration (d) and the entrance aperture diameter (D). There is an MTF difference of more than 17 points between obscured and unobscured optical system operating at IRS TES camera frequency ($x = 0.35$).

used compression technique is discrete cosine transform. The complexity measures in the column [$C_{\text{col}}(f)$] and row [$C_{\text{line}}(f)$] direction of an image are measures of the variance in the image given by,

$$C_{\text{col}}(f) = \frac{1}{(M-1)N} \sum_{i=0}^{M-2} \sum_{j=0}^{N-1} f(i+1, j) - f(i, j),$$

$$C_{\text{line}}(f) = \frac{1}{M(N-1)} \sum_{i=0}^{M-1} \sum_{j=0}^{N-2} f(i, j+1) - f(i, j),$$

where M is the no. of rows and N the no. of columns,
 $1 \leq i \leq M, \quad 1 \leq j \leq N.$

Table 3 shows variation in RMS error with complexity for a constant compression ratio. Higher the complexity measure of the image, less is the spatial redundancy (correlation) in the image. In other words, compression ratio of the image will be less for a given mean square error of the decompressed image. To achieve higher compression ratio for given complexity measures in the row and column direction of an image, one has to tolerate higher loss (i.e. higher mean square error) in the decompressed image.

Indian imaging system: the technology evolution

ISRO started its Earth observation activities through the development and launch of BHASKARA satellite in 1979. This programme which started in 1975 as Satellite for Earth Observation, was based on the frame imaging sensor mounted on a spin stabilized satellite. This modest beginning in Earth observation through two spectral channels producing an image of $341 \times 341 \text{ km}^2$ with a spatial resolution of 1 km heralded the beginning of space-based imaging activities in ISRO. This imaging system made use of vacuum tube version SUPER-VIDICON sensor coupled to an image intensifier as the detecting element. The optical system consisted of multi-element lenses with a focal length of 17 mm and field-of-view of 50 degrees. The electronics was built around analogue components and CMOS technology digital components. The maximum data rate transmitted was only about 91 kilobits/s. From this modest beginning, ISRO has covered large ground in many areas of mastering the imaging technology, utilizing the state-of-the-art technology, and in the process established an excellent base both in human resources and techno-

logy. The successful launch of Technology Experiments Satellite which is providing imagery in panchromatic band with a spatial resolution of 1 m, has enabled ISRO to improve spatial resolution by three orders within a span of two and a half decades.

Imaging technology

ISRO has built imaging instruments, which make use of frame imager (BHASKARA TV payloads), and whiskbroom imagers (INSAT VHRR) flown on a number of INSAT missions and pushbroom imagers (LISS) flown on IRS series of satellites. In addition, the recent TES saw the use of STEP and STARE imaging technology adopted to achieve higher resolution.

Resolution

The spatial resolution has improved from the initial 1 km to 1 m. This has been achieved by innovative system design. When IRS-1C was launched in 1995, the 5.8 m resolution PAN camera was the highest spatial resolution civilian system in the world.

Optics

The use of optical systems for realization of these imaging systems has grown from small focal length of 17 mm to 3920 mm in TES. From predominantly importing optical systems during the initial programmes, ISRO adopted new and innovative design approaches to take advantage of enabling technologies emerging in the optical fabrication and evaluation areas to provide continuously improved spatial, spectral, radiometric and temporal resolution. ISRO has now reached a stage of realizing majority of its on-board optical systems within the country for both refractive and reflective optical systems. Optics used in TES is totally indigenously built.

Detector

ISRO quickly transited from the vacuum tube technology to all solid state CCD devices because of obvious advantages. Early adoption of the emerging pushbroom technology enabled ISRO to reach a pre-eminent place in the international arena of remote sensing data providers.

Electronics

As the payload resolutions, namely spatial, spectral, radiometric and temporal continuously improved, the demand on electronics system continuously grew. The challenges of higher speeds were progressively overcome by the use of appropriate technology components.

Table 3. Variation in RMS error with complexity for a constant compression ratio

| Column complexity | Line complexity | Compression ratio | RMS error |
|-------------------|-----------------|-------------------|-----------|
| 6.87 | 6.41 | 3.2 | 1.41 |
| 8.56 | 7.91 | 3.2 | 1.84 |
| 13.52 | 13.62 | 3.2 | 2.24 |
| 37.77 | 33.78 | 3.2 | 7.05 |

Data rate

The increasing imaging sensor complexity and ever-increasing resolution demands have contributed to increase in data transmission rate from a modest 91 kilobits/s to 200 megabits/s. The transmission chain capability has grown from VHF to S band to X band systems. The transmission system has also incorporated various types of passive and active phased array antennae for achieving the requisite performance.

Platform

The growing challenges of payloads on platform have been effectively met by designing and developing satellites of progressively higher performance complexities. The BHASKARA satellite was spin-stabilized and this imposed constraints on imaging. The IRS series of satellites are three-axes stabilized. A significant stage has been achieved in design and development of satellite platforms through TES, a forerunner of agile satellites, that have become essential for high resolution imaging capability. The agile satellite enables the sensors to view larger areas (compared to the nadir viewing) within which imageries can be taken.

Thus, ISRO has made rapid strides in imaging technology from space and the technology is at par with global

capability within a period of less than two and half decades (Figure 23). A number of newer technologies in all the above areas are under development to realize improved sensors to meet the needs of the user community for various applications.

Areas of future research

As we move forward improving resolution in spatial, spectral, radiometric and temporal arena, there is a lot to be done both in the area of basic sciences and technology. Some of the frontier areas of future research and development include:

- Radiative transfer models to have better atmospheric correction
- Classification algorithms to improve classification accuracies
- New approach in artificial intelligence and expert systems, especially to take account of features other than spectral difference
- Improved algorithm for retrieval of geophysical and biophysical parameters
- Data compression techniques
- Ultra-lightweight mirrors and adaptive optics
- Optical materials
- Detector arrays with built-in read-out in the infrared region.

| SATELLITE (Launch date) | BHASKARA 1/2 (1979/1981) | IRS – 1A/1B (1988/1991) | IRS 1C/1D (1995/1997) | TES (2002) |
|----------------------------|-----------------------------|----------------------------------|--------------------------|--|
| IMAGING TECHNOLOGY | FRAME IMAGER | PUSH-BROOM | | STEP & STARE |
| SPATIAL RESOLUTION | 1000 m (~80 m)* | 72/36 m (20 m)* | 5 m (10 m)* | 1 m (1 m)* |
| OPTICS FOCAL LENGTH | REFRACTIVE (10-350 mm) | | REFLECTIVE (~980 mm) | CATADIOPTIC (~3920 mm) |
| DETECTOR | VIDICON/ VACUUM TUBE | LINEAR ARRAY CCD/SOLID STATE | | |
| ELECTRONICS | CMOS | LSTTL/STTL | FTTL/STTL | |
| DATA RATE | ~100 Kbps | 5-20 Mbps | ~100 Mbps | ~200 Mbps |
| PLATFORM | SPIN-STABILISED | 3-AXIS STABILISED/ SUN-SYNCH. | | 3 AXIS STABIL. /SUN SYNCH. AGILE |

*International civilian earth observation satellite spatial resolution capability during the period

Figure 23. Schematics showing the technology evolution of Indian satellite-borne imaging system for Earth resources survey.

Concluding remarks

I may mention that these and many other scientific and technological themes provide extremely interesting and exciting opportunities for research and development. Currently, ISRO is supporting several of the activities related to the above, in a number of academic, and research and development institutions. I am sure the fellow academic community assembled here would take advantage of many of these opportunities, as the funding support can be made available for such frontier research activities.

Before I conclude, it is my privilege to recall the extensive work of the Founder of the Academy, C. V. Raman, in the fundamental areas of optics and spectroscopy using instruments built by himself, which ultimately led him to the Nobel Prize. Today, in the context of the newly emerging areas of remote sensing from space and also research in astronomy, there is a resurgence in the activities related to optical instrument development. Further, the constraints of building a satellite, with limited volume and weight have resulted in innovative approaches to the design of the optical system for the telescopes, some of which have been described here. This in turn, has resulted in the realization of world-class optical engineering and technology capability in India. Through these recent achievements, we pay our own humble tributes to the pioneering role played by Raman in the development of optic sensors and spectroscopic techniques in India.

1. Kidder, S. Q. and Vonder Haar, T. H., *Satellite Meteorology*, Academic Press, San Diego, 1995, pp. 66–68.
2. Campbell, J. B., *Introduction to Remote Sensing*, Taylor and Francis, London, 1996, pp. 35–37.
3. Sabins, F. F., *Remote Sensing Principle and Interpretation*, Freeman and Co, 1987, 2nd edn.
4. Liou, K. N., *An Introduction to Atmospheric Radiation*, Academic Press, Orlando, 1980, pp. 6–9.
5. Chandrasekhar, S., *Radiative Transfer*, Dover Publication, New York, 1960, pp. 8–14.

6. Indrani Das, Mohan, M. and Krishnamoorthy, K., Detection of marine aerosols with IRS P4-Ocean Colour Monitor. *Proc. Indian Acad. Sci. (Earth Planet. Sci.)*, 2002, **III**, 425–435.
7. Sarangi, R. K., Prakash Chauhan, Mohan, M., Nayak, S. R. and Navalgund, R. R., Phytoplankton distribution in the Arabian Sea using IRS-P4 OCM satellite data. *Int. J. Remote Sensing*, 2001, **22**, 2863–2866.
8. Doerffer, R., Imaging spectroscopy for detection of chlorophyll and suspended matter. In *Imaging Spectroscopy: Fundamentals and Prospective Applications* (eds Toselli, F. and Bodechtel, J.), Kluwer, Dordrecht, 1992, pp. 215–257.
9. Prakash Chauhan, Nagur, C. R. C., Mohan, M., Nayak, S. R. and Navalgund, R. R., Surface chlorophyll *a* distribution in Arabian Sea and Bay of Bengal using IRS-P4 Ocean Colour Monitor satellite data. *Curr. Sci.*, **80**, 127–129.
10. Gordon, H. R., Atmospheric correction of ocean colour imagery in the earth observation system era. *J. Geophys. Res.*, 1997, **102**, 17081–17106.
11. Prakash Chauhan, Mohan, M. and Nayak S. R., Comparative analysis of ocean colour measurements of IRS-P4 OCM and SeaWiFS in the Arabian Sea. *IEEE Trans. Geosci. Remote Sensing*, 2003, **41**, 922–926.
12. George Joseph, *Fundamentals of Remote Sensing*, Universities Press (India), Hyderabad, 2003, pp. 43–44.
13. National Research Council, *Tactical Display for Soldiers: Human Factors*, National Academy Press, Washington DC, 1997.
14. George Joseph, Imaging sensors for remote sensing. *Remote Sensing Rev.*, 1996, **13**, 257–342.
15. Gerald, C. H., *Electro-Optical Imaging System Performance*, JCD Publishing, Winterpark, FL, USA and SPIE Optical Engineering Press, WA, USA, 1995.
16. Rafael, C. G. and Richard, E. W., *Digital Image Processing*, Addison-Wesley, Reading, MA, 1992.
17. Randy Crane, *A Simplified Approach to Image Processing*, Prentice Hall, USA, 1997.

ACKNOWLEDGEMENTS. I thank Dr George Joseph for assistance in the preparation of the manuscript. I would also like to acknowledge the use of material from his book *The Fundamentals of Remote Sensing*, wherever relevant. I thank A. S. Kiran Kumar, Dr J. V. Thomas and Mukund Rao for fruitful discussions that shaped my own thoughts in structuring this manuscript.

Received 2 June 2004; revised accepted 12 July 2004